Physiology in Press; published online on July 7, 2005 as 10.1113/jphysiol.2005.086793

Factors mediating powerful voltage attenuation along CA1 dendrites

Nace L. Golding, Timothy J. Mickus, Yael Katz, William L. Kath and Nelson Spruston

Dept. of Neurobiology & Physiology, Institute for Neuroscience, Northwestern University, Evanston, IL 60208.

Running title: Voltage attenuation in CA1 dendrites

Correspondence to:

Dr. Nelson Spruston

2205 Tech Dr.

Evanston, IL 60208-3520

tel: (847) 467-2734

fax: (847) 467-4898

email: spruston@northwestern.edu

183 words in abstract

36 pages text

7 figures

3 tables

Abstract

We performed simultaneous patch-electrode recordings from the soma and apical dendrite of CA1 pyramidal neurons in hippocampal slices, in order to determine the degree of voltage attenuation along CA1 dendrites. 50% attenuation of steady-state somatic voltage changes occurred at a distance of 238 μm from the soma in control and 409 μm after blocking the hyperpolarization-activated (H) conductance. The morphology of three neurons were reconstructed and used to generate computer models, which were adjusted to fit the somatic and dendritic voltage responses. These models identify several factors contributing to the voltage attenuation along CA1 dendrites, including high axial cytoplasmic resistivity, low membrane resistivity, and large H conductance. In most cells the resting membrane conductances, including the H conductances, were larger in the dendrites than the soma. Simulations suggest that synaptic potentials attenuate enormously as they propagate from the dendrite to the soma, with greater than 100-fold attenuation for synapses on many small, distal dendrites. A prediction of this powerful EPSP attenuation is that distal synaptic inputs are likely only to be effective in the presence of conductance scaling, dendritic excitability, or both.

Introduction

The complex processing of synaptic inputs that occurs throughout a neuron greatly depends on the passive membrane resistivity (R_m) of the neuronal membrane and the internal resistivity (R_i) of the dendrites. These properties, together with dendritic morphology, provide the foundation upon which synaptic integration and action potential initiation take place. Despite their importance, we know little about the values of these parameters, in part because they are difficult to estimate on the basis of somatic recordings. As a result, we do not know how many distal synaptic inputs are needed to trigger an action potential, because the amount of depolarization they produce and the extent to which they attenuate on their way to the soma are not known. Likewise, we cannot predict with precision the time course over which synaptic potentials, when generated in dendrites, will summate in the soma and axon. One way to address these problems is to develop accurate computer models of neurons. These require, however, that we determine the electrical properties of dendrites.

R_i is a particularly important determinant of dendritic voltage attenuation, but it is notoriously difficult to estimate. Modeling somatically recorded voltage responses in compartmental representations of reconstructed neurons has led to estimates ranging from 50 Ωcm to over 400 Ωcm (Rall, 1959; Barrett & Crill, 1974; Durand *et al.*, 1983; Shelton, 1985; Clements & Redman, 1989; Major *et al.*, 1994; Rapp *et al.*, 1994; Thurbon *et al.*, 1994; Thurbon *et al.*, 1998; Chitwood *et al.*, 1999). Other techniques, such as recording with voltage-sensitive dyes (Meyer *et al.*, 1997) or dendritic patch-electrode recording (Stuart & Spruston, 1998) have been used to measure voltage attenuation, thus constraining estimates of R_i. Here we describe the results of experiments using simultaneous somatic and dendritic recordings to measure directly the voltage attenuation from the soma to the apical dendrites of CA1 pyramidal neurons. We also

used three-dimensional morphological reconstructions of three neurons and their voltage responses to estimate the resting membrane properties and R_i in these neurons. We observed dramatic voltage attenuation in CA1 dendrites, which was attributable to high R_i and a leaky dendritic membrane, in part due to substantial resting activation of the hyperpolarization-activated (H) conductance. The resulting computer models of CA1 neurons offer insight into important aspects of synaptic integration in the hippocampus.

Materials and methods

All experimental protocols were approved by the Animal Care and Use Committee of Northwestern University.

Slice preparation and recording: Hippocampal slices (300 μm thick) were prepared from 4-10 week old male Wistar rats (average age 47 days old with only one cell at 28 days old). The rats were anesthetized with halothane, and perfused transcardially with ice-cold artificial cerebrospinal fluid (ACSF). Brains were removed in cold ACSF, blocked for slicing, and placed into the slicing chamber in cold, oxygenated ACSF. Slices were cut in 300 μm sections using a Leica VT 1000S tissue slicer (Leica Instruments, Heidelberg, Germany). Slices were then transferred to a holding chamber filled with oxygenated ACSF, and stored at 35˚C for 30-60 minutes, and subsequently held at room temperature. Slice quality was optimal for approximately 4 hours.

Slices were visualized with infrared differential interference microscopy (Stuart *et al.*, 1993) using a fixed-stage microscope (Zeiss Axioscop, Carl Zeiss Inc., Thornwood, NY) and a Newvicon tube camera (Dage-MTI, Michigan City, IN). Glass electrodes (glass type EN-1, Garner Glass, Claremont, CA) were pulled and fire-polished (Flaming/Brown P97 puller, Sutter

Instruments, Novato, CA) to 4-9 MΩ resistance as measured in the bath. Simultaneous recordings from the soma and the primary apical dendrite were done in the whole-cell patch-clamp mode under visual control. Seal resistances were greater than 2 GΩ. Recordings were made at temperatures of 34-37˚C.

Solutions: ACSF contained (in mM): 125 NaCl, 2.5 KCl, 25 $NaHCO_3$, 1.25 NaH_2PO_4, 1 $MgCl_2$, 2 $CaCl_2$, 25 dextrose. The ACSF was bubbled with a 95% O_2-5% CO_2 gas mixture to oxygenate the solution and maintain a pH of 7.4. Pipette solution contained (in mM): 115 potassium gluconate, 20 KCl, 10 sodium phosphocreatine, 10 HEPES, 2 Mg-ATP, 0.3 Na-GTP, 2 EGTA, and 0.1% biocytin, pH 7.35 with KOH. Most experiments were done in the presence of 30 µM D-AP5 (Precision Biochemicals), 1-2 µM CGP55845A (a gift from Novartis Pharmaceuticals, East Hanover, NJ) and 1-5 µM SR-95531 (Sigma/RBI) to block all but fast excitatory synaptic transmission. ZD7288 (Tocris, Balwin, MO) was made as a 5 mM stock solution in distilled water and diluted to a final concentration of 50-100 µM. CsCl (Sigma, St. Louis, MO) was added directly to the ACSF to obtain a final concentration of 5 mM.

Data-acquisition: Current-clamp recordings were made using identical BVC-700 patch-clamp amplifiers (Dagan Instruments, Minneapolis, MN) with bridge balance and capacitance compensation employed. Electrophysiological records were filtered at 5 kHz and digitally sampled at 10-50 kHz. Data were acquired using Macintosh computers (Apple, Cupertino, CA) and an ITC-16 or ITC-18 interface (Instrutech, Great Neck, NY), using custom macros running under Igor Pro (WaveMetrics, Lake Oswego, OR). Hyperpolarizing pulses were injected into the soma with two different step sizes. First, a long pulse was delivered that caused less than 5 mV deflection from the resting potential (generally 30-50 pA). This was followed by a 1 ms, 1.5 nA hyperpolarizing current injection. This protocol was repeated at least 20 times and

trials were averaged. The bridge balance was carefully monitored throughout each experiment. After the experiment was over, the electrodes were slowly withdrawn to achieve the outside-out patch configuration. Slices were then placed into 4% paraformaldehyde solution and stored until histology was performed (about 1 week later).

Data analysis: All analysis was done using IGOR Pro software. Steady-state attenuation and input resistances were measured over the last 30 ms of a 400 ms hyperpolarizing current pulse. As all CA1 pyramidal cells investigated showed a "sag" response from the H current (Maccaferri *et al.*, 1993; Magee, 1998), input resistances were measured in the presence of 5 mM CsCl or 50-100 µM ZD7288. In control solution we measured the sag ratio for both somatic and dendritic responses, where sag ratio is defined as the steady-state membrane potential divided by the peak potential. Time constants were measured at both the onset (τ_{ON}) and offset (τ_{OFF}) of the long hyperpolarizing voltage response, as well as the offset response following the short-duration current pulses (τ_{SHORT}) for cells bathed in 5 mM CsCl. To minimize contamination of voltage-dependent processes that developed during the current protocol, we also compared τ_{ON} and τ_{OFF} (Spruston & Johnston, 1992). If either time constant was greater than 20% different from the average (of the on and off responses) the neuron was not included in the analysis (8 out of 39 cells were rejected, yielding 31 cells in the final data set). The three cells that were modeled had time constant differences (τ_{ON} vs. τ_{OFF}) of 1.3, 2.2, and 13%. Pooled data are reported as mean ± SEM. All statistical unpaired t-tests used a significance level of 0.05.

Histology and neuronal reconstructions: Neurons were visualized using the DAB reaction (Vectastain ABC kit, Vector Laboratories Inc., Burlingham, CA) using standard procedures. No clearing or dehydration was used in order to prevent shrinkage of slices. After histology, slices were mounted in aqueous mounting medium (Moviol, Calbiochem, LaJolla,

CA). We checked for shrinkage by comparing images and measurements taken from the both the microscope and monitor during the experiment to the diameters measured in the fixed slice, and no shrinkage of diameters was seen. There was no apparent change in length of the neurons, as there was no difference between inter-electrode distance measured during the experiment and on the fixed sections.

Neurons were selected for reconstruction based on three criteria: 1) robust staining of the dendritic tree, 2) an absence of any obviously cut dendrites, 3) attenuation of steady-state voltage responses was within one standard deviation of the mean linear fit of attenuation vs. distance (see Fig. 2). The three cells selected for reconstruction were from one 57 day-old rat (cells 1 and 2 in Fig. 1) and one 55 day-old rat (cell 3); all three cells had somata within stratum pyramidale. Cells were reconstructed using a Zeiss inverted microscope (63x oil immersion objective) fitted with semi-automated Neurolucida hardware and software (version 2.1, MicroBrightField Inc., Colchester, VT). This allowed us to reconstruct the three-dimensional position and diameter of the dendritic branching pattern. The Neurolucida file was then converted to a NEURON geometry file by the Neuroconvert program (version 2.0b4, D. Niedenzu and G. Klein, MPI für medizinische Forschung, Heidelberg, Germany, 1998). Diameters and lengths in the resulting NEURON models were then compared to those of the fixed slice for accuracy. Spine density was accounted for based on density measurements from Megias et al., who showed that spines on CA1 neurons are nonuniformly distributed (Megias *et al.*, 2001). This spine distribution was checked and agreed well with the actual spine distribution in the neurons we reconstructed. We also found that our spine distribution agrees with other published accounts (Bannister & Larkman, 1995b). Each model was divided into regions matching those described by Megias et al., and we calculated the increased area due to the reported spine density in each region, (based

on average spine area of 0.83 μm^2; Harris & Stevens, 1989). Taking the ratio of the areas with and without spines gave us a "spinescale" variable for each dendritic region, which ranged from 1.0 (for regions with no spines) to 3.3 (in locations with thin dendrites and many spines, especially the thin dendrites of stratum radiatum). We accounted for this extra area in the models by dividing R_m and multiplying C_m (initially 1.0 $\mu F/cm^2$; see Gentet *et al.*, 2000) by the appropriate spinescale parameter (Holmes, 1989; Bush & Sejnowski, 1993; Stuart & Spruston, 1998). The spines contributed extra areas of 23,241 μm^2, 23,279 μm^2, and 22,798 μm^2 in the three reconstructed neurons, corresponding to an average of 54% of the total membrane area. The geometry of the soma was also adjusted to account for deviations from the cylindrical compartments used in models. We assumed an ellipsoid soma for the cross section of the soma, which resulted in multiplying the diameters of the somatic compartment by 0.77 to make them equivalent to an ellipse.

Because reconstructing the surface area of neurons is imprecise, deviations from the standard C_m value of 1.0 $\mu F/cm^2$ (see Table 3) could reflect errors in surface area estimates. Hence one could argue that C_m should be adjusted from a hypothetical best-fit value of 1.5 $\mu F/cm^2$ down to the standard value of 1.0 $\mu F/cm^2$. To do this, however, a surface-area scaling factor of 1.5 would then be applied to R_m and C_m (as described for spine scaling, above) and the resulting model would be mathematically identical to the original.

Simulations: Simulations were performed using the NEURON simulation environment (Hines & Carnevale, 1997) on Macintosh computers using a time step of 0.1 ms. We used the built in run-fitter function to directly fit the voltage responses at both the soma and dendrite. This fit routine used a minimization of the mean-square error to determine the best fit. R_i, C_m, and R_m were allowed to vary independently. Leak potentials were set at the resting potential of the

neuron in the presence of 5 mM CsCl (-66, -72, and -69 mV for the three cells modeled). Simulated fast excitatory synaptic conductances were modeled using a two-exponential function, with τ_{rise}=0.5 ms and τ_{decay}=5.0 ms. The reversal potential for the synaptic current was set to 0 mV. We used the same sigmoid function strategy as Stuart and Spruston (1998) to model both the nonuniform R_m gradients. For each section,

$$R_m = R_m(end) + \frac{R_m(soma) - R_m(end)}{1 + e^{(dis_{half} - dis)/steep}} \qquad \text{Equation 1}$$

where $R_m(soma)$ is the R_m at the soma, $R_m(end)$ is the R_m at the end of the apical dendrites, dis_{half} is the distance at which the function is at halfway between the somatic and end values, and *dis* is the distance from the soma. The *steep* variable set the steepness of the transition from $R_m(soma)$ to $R_m(end)$.

The H conductance (G_h) was similar to the one used by Stuart and Spruston (1998), but was modified to reflect measurements of H current in CA1 (Magee, 1998). The reversal potential, based on the measured permeabilities to Na^+ and K^+ and our ionic concentrations, was set to -25 mV (Magee 1998). The kinetics of the H conductance were described by a first-order gating variable with forward (α) and reverse (ß) rate constants described by the equations:

$$\alpha = \alpha_0 * \exp(azFV/RT) \qquad \text{Equation 2}$$

$$ß = \alpha_0 * \exp([1-a]zFV/RT) \qquad \text{Equation 3}$$

where z=7 is the steepness of the steady-state activation curve, which is given by $\alpha/[\alpha+\beta]$, and a=0.4 is an asymmetry factor for the activation and deactivation time constants, which are given by $\tau=1/(a[\alpha+\beta])$. α_0 is the rate constant at the half-activation voltage, V (volts) is the difference between the membrane potential (V_m) and the half-activation voltage ($V_{1/2}$ = -81 mV; Magee 1998). F is the Faraday constant (96,485 $Cmol^{-1}$), R is the gas constant (8.315 $Jmol^{-1}K^{-1}$), and T

is temperature (K). α and ß were further scaled by a common factor to optimize fits of the data. The resulting scale factors yielded time constants similar to those published by Magee (1998).

The distribution of H conductance as a function of distance from the soma was modeled using a sigmoidal function. For each section,

$$G_h = G_h(soma) + \frac{G_h(end) - G_h(soma)}{1 + e^{(dis_{half} - dis)/steep}} \qquad \text{Equation 4}$$

where $G_h(soma)$, $G_h(end)$, dis_{half}, dis, and $steep$ have meanings similar to equation 1 (see Discussion for justification). As for the nonuniform membrane resistivity, the run-fitter in NEURON was used to find the parameters that minimized the difference between the simulated and actual data.

In all instances where the run-fitter was used, the steady-state voltage response was weighted heavily in order to ensure optimal fitting of steady-state voltage attenuation. In addition, for each data set fit, multiple fits were performed using different starting values and the fit with the lowest mean-square error was chosen. This strategy reduces the likelihood that a substantially better fit would be missed due to local minima in the parameter space. To validate the parameter search algorithm used in the run fitter, we attempted to re-fit simulated data and compared the resultant best-fit parameters to the original parameters used to generate the data. Specifically, we added Gaussian noise (0.02 mV RMS) to a simulated hyperpolarizing voltage response with sag and re-fit it the resulting data with the nonuniform G_h distribution described above. Five fits with different starting values yielded parameters that were on average 16% different from the parameters used to generate the data. The best of the five fits yielded parameters only 7% different from the values used to generate the data. Despite this difference, each of the five fits had an error of only 0.05 mV.

[Note: All code for reproducing the computer simulations described in this paper will be made publicly available at the lab web site after acceptance for publication. We have already shared the code for our reconstructed pyramidal neurons with several investigators.]

Results

Direct measurements of voltage attenuation

We measured the attenuation of voltage, in the somatic to dendritic direction, along the primary apical dendrite of CA1 hippocampal pyramidal neurons, by using simultaneous somatic and dendritic whole-cell, patch-pipette recordings in brain slices from adult rats. Both long and short current injections (-30 to -50 pA for 400 ms; -1.5 nA for 1 ms) were made at the somatic electrode, and the corresponding voltage responses were measured at both recording locations (Fig. 1). Somatic electrodes had lower series resistance (<40 MΩ) than dendritic electrodes (<90 MΩ). We therefore limited our experiments to consideration of voltage attenuation from the soma to the dendrite, as dendritic current injection produced larger voltage errors due to the higher series resistance. We also limited responses to small hyperpolarizations, in order to minimize activation of voltage-gated conductances. Nevertheless, every cell exhibited a "sag" repolarization (Fig. 1B) during the long pulse, due to the presence of the H conductance (Maccaferri *et al.*, 1993; Magee, 1998). Application of 5 mM CsCl (n=13) or 50-100 µM ZD7288 (n=5) to the bath blocked the sag in both the somatic and dendritic responses (Fig. 1C).

The average input resistance (R_N) of the pyramidal neurons in control ACSF was 54±2 MΩ and the sag ratio was 0.83±0.01 (n=31). In cells where CsCl or ZD7288 was applied following control, the input resistance more than doubled, from 54±3 MΩ to 109±8 MΩ (n=13), and the sag ratio approached one 0.83±0.01 to 0.97±0.0 (n=13), indicating that the H conductance is active at resting potentials (Spruston & Johnston, 1992). Overall, there was a 2-3

fold range of input resistances within both control and CsCl conditions (Table 1), indicating that CA1 neurons may have somewhat heterogeneous electrical properties.

Figure 2 shows steady-state attenuation plotted as a function of distance in both control (*n*=31) and 5 mM CsCl (*n*=13) or 50-100 µM ZD7288 (*n*=5). When fit with a linear function, the half-attenuation distance was 238 µm in control conditions. Attenuation was greatly reduced in the presence of H conductance blockers, with the half-attenuation distance increasing to 409 µm in 5 mM CsCl.

Simulations with nonuniform membrane properties

Three cells were fully reconstructed morphologically (Fig. 1A) and were used to examine the passive membrane properties that could lead to the observed voltage attenuation. We first tested whether models with a uniform membrane conductance would fit the data with the H conductance blocked. Initially we fit only the long-pulse response and then used the resulting best-fit parameters to simulate the short-pulse response. This approach gave poor fits of the short-pulse data. Similarly, when fitting the short-pulse response alone, we obtained poor fits of the long-pulse data (not shown). To compromise, we fit both pulses simultaneously, so as to better constrain our model using both sets of data. As seen in Figure 3, using a uniform membrane conductance could fit the steady-state attenuation, but would not adequately fit the time course of long and short pulses. In particular, the somatic time constants of the models were too fast, and the dendritic time constants in the model were too slow. These differences in time course of the on and off responses suggest a nonuniform distribution of the membrane conductance. We thus allowed the membrane conductance model to vary as a function of distance from the soma using a sigmoid distribution function (see Methods).

Using a nonuniform membrane conductance gave us slightly better fits (see mean square errors of Table 3). Compared to the uniform simulations, the nonuniform model resulted in reductions of the mean square error of the fit for all three cells (35%, 19%, and 12% for cells 1, 2, 3, respectively; average of long- and short-pulse fit errors; see Table 3). Although we were able to match the steady-state attenuation of the long-pulse response at both the somatic and dendritic locations, fits of the voltage relaxations revealed noticeable differences from the experimental data. Specifically, the model responses decayed too rapidly in the soma and too slowly in the dendrites. Fits of the short-pulse responses were also different, with the time to the peak of the dendritic voltage response faster in the model than in the experimental data. We tried other types of functions (such as linear functions or keeping a uniform conductance in the basal dendrites), and varied the fitting parameters but these changes did not result in better fits (not shown).

The models suggest that a nonuniform R_m, where the somatic R_m is greater than the dendritic R_m, could exist in CA1 pyramidal neurons. The values of the R_m distributions required to fit the data varied between cells. For cell 1, the somatic R_m value was two times greater than the dendritic R_m value. In cells 2 and 3, the somatic R_m value was seven times greater. The models also suggest an R_i ranging from 139 to 218 Ωcm, a range substantially higher than that obtained using a similar experimental and modeling strategy in layer V pyramidal neurons (Stuart & Spruston, 1998). In two of the three cells, estimates of C_m are different from the standard value of 1.0 μF/cm^2 (Gentet *et al.*, 2000). This could reflect a real biological variability in C_m, or it could reflect errors in the precision of our estimates of surface area (including spine estimates). As described in the Methods, this has no impact on the model and thus has no effect on any of our results.

Simulations with I_h

CA1 pyramidal neurons possess voltage-gated conductances, such as the H conductance, that are active at the resting potential (Maccaferri *et al.*, 1993; Magee, 1998). These channels are distributed nonuniformly, increasing in density more than six-fold into the apical dendrites (Magee, 1998). As seen in Figure 2, blocking the H conductance directly affects voltage attenuation. We therefore simulated the voltage attenuation in our models after adding a hyperpolarization-activated conductance and attempted to model the observed attenuation. Initial simulations were attempted using a uniform H conductance. As seen in Figure 4A, uniform H-conductance gradients predicted too little steady-state voltage attenuation in two of the three modeled neurons. We therefore allowed the conductance to vary as a sigmoidal function of distance from the cell in the apical dendrites (see Discussion). Using such a nonuniform distribution accurately predicted the observed voltage attenuation in all three cells (Fig. 4B), leading to improved fits compared to the uniform distribution. As shown in Figure 4C, however, the shape of the gradient was different in each cell. Data from cells 2 and 3 were best fit increasing gradients of the H conductance in the dendrites (largest in cell 3), while data from cell 1 was best fit with a gradually decreasing gradient. Furthermore, fully accurate fits of the time course of voltage sag in the responses were not achieved (Fig. 4A,B).

As a test of how well our models simulated our complete experimental data set, we simulated the steady-state voltage attenuation that occurs along the main apical dendrite in each of the models (Figure 5). Using the parameters determined as described above, with no further adjustments, the simulation data fell well within the scatter of the experimental results, both with the H conductance blocked (Fig. 5A) and not blocked (Fig. 5B).

Attenuation of synaptic potentials

We next used our models to make predictions about the attenuation of synaptic potentials from their origin to the soma. To test the ability of our models to accurately predict EPSP attenuation, we compared the attenuation observed in the models to that observed in experiments (Fig. 6). Synapses in the distal apical dendrites were activated via a stimulating electrode placed in stratum lacunosum-moleculare and the resulting EPSPs were recorded simultaneously in the soma (1-6 mV) and the apical dendrite (6-19 mV, n=6, 242-390 μm from the soma). Attenuation of the EPSP is presented by plotting the ratio of the peak EPSP amplitude in the soma to the amplitude measured in the dendrite ($V_{soma}/V_{dendrite}$). In the model, a distal synaptic input was simulated with forty inputs distributed in the apical dendritic tuft, each with the unitary synaptic conductance of 0.1 nS, a rise time constant of 0.5 ms and a decay time constant of 5 ms, yielding composite somatic EPSPs of 1.8 to 3.6 mV (in the three models). Simulations and experiments were both performed with the H conductance present. The model data are plotted as $V_{soma}/V_{dendrite}$ for dendritic locations along the main apical dendrite. As shown by the plot in Figure 6B, the simulations are in good agreement with the experimentally determined EPSP attenuation along the main apical dendrite.

These results indicate that synaptic potentials are subject to substantial attenuation as they propagate from the apical dendrites toward the soma. For example, about three-fold attenuation was predicted and observed from a point about halfway along the main apical dendrite to the soma (300 μm). Even more attenuation is to be expected, however, between the site of the synapses (mostly on small branches inaccessible to patch-clamp recording) and the main apical dendrite. The total amount of attenuation was therefore predicted using the model. Using cell 3, we simulated fast EPSPs at five different synaptic locations to determine the resulting voltage

attenuation. For example the basal synaptic input only 135 μm from the soma attenuated more than 40 fold, from an EPSP of 12.4 mV at the synapse to 0.3 mV at the soma. The synapse on the main apical dendrite produced a similar somatic EPSP, although the EPSP at the synapse was much smaller (about 1 mV) and attenuation is less severe (about 4 fold) because of the large diameter of the main apical dendrite. This illustrates that both the amplitude of the EPSP at the synapse and its attenuation to the soma are inversely related to the diameter of the dendrite. Synapses on small diameter dendrites off the soma (e.g. basal synapse) produce large EPSPs that attenuate dramatically, whereas synapses on larger dendrites yield smaller EPSPs that attenuate less (e.g. main apical synapse). These two factors oppose each other, leading to so-called "passive normalization of EPSPs" (Jaffe & Carnevale, 1999). Because apical oblique dendrites are smaller, synapses on these dendrites produce larger local EPSPs subject to more attenuation. For the apical oblique synapse shown in Figure 7 (purple marker), the local EPSP is large (8.4 mV), but attenuation is severe (34 fold), yielding a small, 0.25 mV EPSP at the soma. Much of this attenuation occurs at the connection point between the small-diameter oblique branch and the larger-diameter main apical dendrite (13 fold), with a smaller attenuation between this site and the soma (2.5 fold). Each of these three synapses considered so far (basal, main apical, and apical oblique) produces similar somatic EPSPs (0.25-0.3 mV), but EPSPs become substantially smaller for more distal synaptic locations, such as those on the distal apical tuft. Two examples are shown in Figure 7 (synapses at orange and yellow markers). These two synapses are quite different, due to the diameter of the dendrite and the distance from the soma. The orange synapse produces a local EPSP of 4.16 mV, which attenuates 26 fold to produce a somatic EPSP of 0.16 mV. The yellow synapse produces a much larger local EPSP (19.8 mV), largely due to the small

diameter of the dendrite, but attenuates much more (330 fold) to yield a very small somatic EPSP (0.06 mV).

Our model, with the H conductance present, predicts that synaptic responses attenuate greatly, even from proximal apical and basal synaptic sites (Fig. 7). Some of this attenuation may be attributable to the high density of the H conductance in the apical dendrites (Magee, 1998), so we examined the effects of the H conductance on synaptic attenuation in the model. For all synapses shown in Figure 7, removing the H conductance from the model reduced attenuation of EPSPs. The effect was greatest, however, for the most distal synapses on the apical dendrites. For the most distal synapse shown, removing the H conductance decreased attenuation from 330 fold to 220 fold.

Discussion

We measured the attenuation of long and transient voltages in CA1 pyramidal neurons in adult rats under conditions in which the hyperpolarization-activated conductance was present or blocked. These experiments indicate that voltage attenuation along the CA1 dendrite is large, especially when the H conductance is not blocked. We also measured the attenuation of synaptic potentials, which undergo considerable attenuation, even along the relatively large primary apical dendrite, and used these measures to inform estimates regarding EPSP attenuation in regions of the dendrites that are too small for recording electrodes.

In addition to these direct experimental measures, compartmental models were developed using morphological reconstructions of three neurons in which we measured somato-dendritic attenuation. These models allowed us to make predictions about how synaptic potentials will sum in the dendrites and propagate toward the soma and axon, where action potential initiation occurs. The availability of experimental data from simultaneous somatic and dendritic recordings

from the reconstructed neurons greatly constrains the models, thus increasing their predictive power.

Powerful voltage attenuation along CA1 dendrites

We found that when the H conductance is present, steady-state potentials attenuate to 50% at a distance of 238 µm from the soma. When G_h is blocked the 50% attenuation distance increases to 409 µm. These 50% attenuation values are substantially shorter than the corresponding measures in layer V neocortical pyramidal neurons (332 µm with G_h present; 536 µm with G_h blocked; Stuart & Spruston, 1998). In addition to differences in morphology (CA1 cells are shorter overall, have smaller diameter apical dendrites, and have more oblique apical side branches), the electrical properties of CA1 dendrites differ from those of layer V pyramidal neurons. Specifically, modeling suggests that three important factors that contribute to voltage attenuation in CA1 dendrites: 1) relatively high values of internal resistivity; 2) a nonuniform gradient of membrane resistivity, in which R_m decreases as a function of distance; and 3) a high, nonuniform density of the H conductance in the dendrites.

High internal resistivity

Our results suggest that the internal resistivity (R_i) of CA1 pyramidal neurons lies within the range of 139-218 Ωcm. This range is consistent with values of R_i reported for other cell types using a variety of methods (Rall, 1959; Barrett & Crill, 1974; Durand *et al.*, 1983; Shelton, 1985; Clements & Redman, 1989; Major *et al.*, 1994; Rapp *et al.*, 1994; Thurbon *et al.*, 1994; Meyer *et al.*, 1997; Stuart & Spruston, 1998; Thurbon *et al.*, 1998; Chitwood *et al.*, 1999), but the range is narrower due to the constraints provided by combined dendritic and somatic recording. Our estimates of R_i for CA1 dendrites are, however, about twice as high as estimates from layer V

pyramidal neurons obtained using similar methods (Stuart & Spruston, 1998), thus raising the interesting possibility that internal resistivity is cell-type dependent.

Although estimates of R_i using our approach are sensitive to the accuracy of the morphological reconstructions (estimation of diameter and spine densities are key factors), the methods used here are virtually identical to those used to estimate R_i in layer V neurons, so morphological errors are unlikely to account for the nearly two-fold different values of R_i.

Our model-based fits of the data did not accurately capture all aspect of the kinetics of long and short current-pulse voltage responses. Most notably, the time to the peak of the dendritic voltage response to short current injections at the soma was generally too short in the model. Lower values of R_i (i.e. closer to estimates from cortical layer V pyramidal neurons) gave even poorer fits of this aspect of the data and produced lower input resistance and too little voltage attenuation. Decreasing R_m (at lower R_i) increased voltage attenuation, but lowered input resistance even further.

It may be incorrect to assume that R_i is constant throughout the entire neuron. For example, smaller branches could have higher internal resistivity than large branches due to "clogging" of the smallest dendrites by organelles with fixed size. Organelles, such as the smooth and rough endoplasmic reticulum, are also distributed nonuniformly throughout the dendrites and spines of CA1 pyramidal neurons, and could potentially affect the internal resistivity of dendritic branches (Krijnse-Locker *et al.*, 1995; Spacek & Harris, 1997). Our attempts to fit our data using models with nonuniform R_i, however, did not yield significant improvements (not shown).

Although our models predict voltage attenuation well, they are not as good at predicting the kinetic filtering of fast membrane potential changes. Because we are confident of the ability

of the fitting algorithm to find a good fit if the underlying function is correct (errors in fits to idealized data, Methods, are much lower than error in fits to actual data, Table 3), such flaws in the fits suggest that our models do not capture precisely the kinetic aspects of voltage changes in the neurons. Thus, factors not included in the model likely affect the time course of synaptic potentials in dendrites. To improve the model, it will likely be necessary to include additional voltage-gated conductances that are active near the resting potential. Such improvements will require additional experimental analysis. Although better models are needed, the conclusion that voltage attenuates powerfully in CA1 dendrites is constrained by direct experimental observation. We tried a large number of variations on the parameters chosen using the "best-fit" approach. Any such model may be considered reasonably valid, provided that it fits the observed somato-dendritic voltage attenuation. With all of these models our conclusions regarding the attenuation of synaptic potentials were robust in demonstrating that EPSPs attenuate dramatically along the length of CA1 dendrites.

Nonuniform membrane resistivity

Our simulations suggest that the membrane resistance is nonuniform in CA1 pyramidal cells, with R_m decreasing as a function of distance, making distal dendrites "leakier" than proximal dendrites. The function describing R_m with distance is sigmoidal in our model, a reasonably simple function that can approximate anything from a nearly linear function to a step function. Our fitting routine arrived at intermediate distributions. We do not claim that the resulting functions are quantitatively accurate descriptions of R_m, which may in reality be very complicated. Rather, we find that our data cannot be fit with gradients in the reverse direction, suggesting that distal dendrites are leakier than the proximal dendrites and soma. The simple function we used does a good job of reproducing accurately the steady-state voltage attenuation

and does a reasonably good job of fitting the time course of somatic and dendritic voltage responses to step currents with G_h blocked.

The suggestion that R_m decreases as a function of distance from the soma is similar to that obtained for layer V neocortical pyramidal neurons (Stuart & Spruston, 1998). We have described the case in which R_m is lower in the dendrites than in the soma, thereby making the dendrites "leakier" than the soma, which increases attenuation compared to the case where the dendritic membrane is equivalent to the somatic membrane. Although we did not block synaptic transmission or neurotransmitter receptors in our experiments, the low level of background synaptic activity in slices is likely to contribute minimally to the resting membrane properties in our experiments. *In vivo*, however, ongoing synaptic activity present is likely to increase the membrane conductance, resulting in dendrites that are potentially "leakier" than what we describe in this work (Bernander *et al.*, 1991; Rapp *et al.*, 1992).

Rather than viewing the dendrites as leakier than the soma, another way of viewing a nonuniform R_m is to compare it to a uniform R_m equal to the average throughout the soma and dendrites. Using this approach, London et al. concluded that the nonuniform R_m case improves voltage transfer of both steady-state and synaptic potentials to the soma (London *et al.*, 1999). Thus, whether a lower R_m in the dendrites is viewed as an advantage or disadvantage is a semantic issue that depends on point of reference. Viewed relative to the low R_m in the distal dendrites, the higher R_m in the proximal dendrites and soma decreases voltage attenuation; viewed relative to the high R_m in the soma and proximal dendrites, the additional leak in the distal dendrites increases voltage attenuation.

Nonuniform H conductance

The H conductance was originally suggested to be increasing in layer V pyramidal neurons based on simulations of voltage attenuation (Stuart & Spruston, 1998). Subsequent cell-attached patch recordings in layer V pyramidal neurons demonstrated that there is an initial, small, linear increase in H current density, followed by a sharp, nonlinear increase in H current density more distally (after about 400 µm), where the density increases by thirteen-fold (Williams & Stuart, 2000; Berger *et al.*, 2001). Similarly, in CA1 pyramidal neurons, an increase in H current density of more than six fold was observed over the first 350 µm of the primary apical dendrite (Magee, 1998). Studies with antibodies to the H-channel subunit HCN-1 suggest that the H conductance increases dramatically (approximately 60 fold) in the more distal apical dendrites of CA1 neurons, while the density in basal dendrites is close to the somatic level (Santoro *et al.*, 1997; Lörincz *et al.*, 2002).

Our simulations support the idea that the H conductance is distributed nonuniformly in CA1 pyramidal neurons. However, the gradients predicted by our models varied considerably amongst the three cells modeled. Two out of the cells exhibited the expected increase in G_h as a function of dendritic distance from the soma, while the third cell actually produced a reverse gradient, with the highest density of G_h in the soma and proximal dendrites. This finding raises that possibility that there may be heterogeneity in the distribution of H channels within the CA1 pyramidal cell population (Bullis *et al.*, 2004). This heterogeneity of CA1 neuron is in keeping with the large range of input resistances and sag ratios observed in the experimental data (Table 1; Staff *et al.*, 2000) as well as the heterogeneity in other properties, such as action potential backpropagation (Golding *et al.*, 2001). Interestingly, cell 1 had a reverse gradient of G_h, the smallest nonuniform R_m gradient, and also had a somewhat atypical morphology, with more

apical oblique dendrites than most CA1 pyramidal neurons (Bannister & Larkman, 1995a). These observations suggest that there may be morphologically and physiologically distinct classes of pyramidal neurons within CA1 (see also Golding *et al.*, 2001).

Attenuation of synaptic potentials

Our simulations predict that EPSPs will attenuate dramatically as they propagate to the soma. Although we constrained the models using the voltage attenuation measured between the soma and the dendrite, the resulting models predicted accurately the EPSP attenuation we measured between the main apical dendrite and the soma (see also Magee & Cook, 2000). Our simulations also indicate that even greater attenuation occurs between the synapses (usually on small branches) and the main apical dendrite, resulting in enormous attenuation between the synapse and the soma. Scaling of synaptic conductance could compensate for this attenuation in some cases (Magee and Cook 2000), but this mechanism may not work for synapses on very distal dendrites. For example, with the H conductance present, modeling the most distal apical synapse shown in Figure 7 (yellow) with a ten-fold larger synaptic conductance (10 nS) increases the somatic EPSP to 0.2 mV, but at this large conductance level the local EPSP is 54 mV, which brings V_m very close to the synaptic reversal potential. Dendritic spikes are likely to be triggered with EPSPs considerably smaller than this. These observations suggests that very distal synaptic inputs, such as those from the perforant path, may have to trigger local spikes in order to be effective at influencing action potential firing in the axon (Golding & Spruston, 1998; Golding *et al.*, 1999).

Our findings also suggest that, because of the dramatic attenuation of distal EPSPs, somatic recordings may be virtually unable to detect synaptic events originating from remote dendritic locations. This could have implications for experiments in which minimal stimulation

protocols are used (such as for “silent synapse” experiments), in that apparently “missing” EPSPs may be present, yet unobserved in somatic recordings. Indeed, using simultaneous dendritic and somatic patch-clamp recordings from CA1 neurons, Magee and Cook observed many synaptic potentials at the dendritic electrode that fail to cause a change in membrane potential at the soma. This was especially true for inputs located more than 200 μm from the soma (Magee & Cook, 2000).

The presence of the H conductance acts to increase the effective electrotonic length of the neuron, which has a prominent effect on EPSP attenuation. This effect was greatest for synapses on small-diameter, distal apical dendrites (Fig. 7). One proposed function for dendritic H conductance is to normalize temporal summation in the soma for synapses at different dendritic locations (Magee, 1999; Desjardins *et al.*, 2003). Interestingly, we found that normalization of temporal summation occurred even in the model of cell 1, which had a reversed G_h gradient (simulation not shown). This suggests that normalization of temporal summation, though clearly mediated by the H conductance, does not necessarily require a somato-dendritic gradient of the channels.

Future Directions

The models described here will serve as a foundation for more elaborate models incorporating a variety of voltage-activated conductances, which can be used to make predictions about voltage changes in locations that are currently inaccessible to experimental techniques. By making the models freely available, we expect them to be useful in a variety of studies. Our hope is that these results will prompt future investigations, both computational and experimental, that will lead to increasingly accurate and detailed models of CA1 neurons and hippocampal circuits and hence a better understanding of hippocampal function.

Acknowledgements

We thank Dr. Martha Bohn and Dr. Bronwen Connor for assistance with the Neurolucida system, Arndt Roth for assistance with the Neuroconvert software, Drs. Michael Hines and Ted Carnevale for assistance with NEURON, and Nathan Staff for helpful discussion and comments on the manuscript. Supported by grants from the NIH (T32-GM-08061 to TJM, F32-NS-10532 to NLG, and R01-NS35180 and R01-NS-46064 to NS and WLK) and NSF (IGERT fellowship to YK). NS-46064 as part of the NSF/NIH Collaborative Research in Computational Neuroscience Program.

References

Bannister NJ & Larkman AU. (1995a). Dendritic morphology of CA1 pyramidal neurones from the rat hippocampus: I. Branching patterns. *J Comp Neurol* **360,** 150-160.

Bannister NJ & Larkman AU. (1995b). Dendritic morphology of CA1 pyramidal neurones from the rat hippocampus: II. Spine distributions. *J Comp Neurol* **360,** 161-171.

Barrett JN & Crill WE. (1974). Specific membrane properties of cat motoneurones. *J Physiol* **239,** 301-324.

Berger T, Larkum ME & Luscher HR. (2001). High I(h) channel density in the distal apical dendrite of layer V pyramidal cells increases bidirectional attenuation of EPSPs. *J Neurophysiol* **85,** 855-868.

Bernander O, Douglas RJ, Martin KA & Koch C. (1991). Synaptic background activity influences spatiotemporal integration in single pyramidal cells. *Proc Natl Acad Sci U S A* **88,** 11569-11573.

Bullis JB, Jones TD & Poolos NP. (2004). H-channel distribution in pyramidal-like principal neurons in stratum radiatum of hippocampus differs from pyramidal neurons. In *Society for Neuroscience,* San Diego, CA.

Bush PC & Sejnowski TJ. (1993). Reduced compartmental models of neocortical pyramidal cells. *J Neurosci Methods* **46,** 159-166.

Chitwood RA, Hubbard A & Jaffe DB. (1999). Passive electrotonic properties of rat hippocampal CA3 interneurones. *J Physiol* **515,** 743-756.

Clements JD & Redman SJ. (1989). Cable properties of cat spinal motoneurones measured by combining voltage clamp, current clamp and intracellular staining. *J Physiol* **409,** 63-87.

Desjardins AE, Li YX, Reinker S, Miura RM & Neuman RS. (2003). The influences of Ih on temporal summation in hippocampal CA1 pyramidal neurons: a modeling study. *J Comput Neurosci* **15,** 131-142.

Durand D, Carlen PL, Gurevich N, Ho A & Kunov H. (1983). Electrotonic parameters of rat dentate granule cells measured using short current pulses and HRP staining. *J Neurophysiol* **50,** 1080-1097.

Gentet LJ, Stuart GJ & Clements JD. (2000). Direct measurement of specific membrane capacitance in neurons. *Biophys J* **79,** 314-320.

Golding NL, Jung HY, Mickus T & Spruston N. (1999). Dendritic calcium spike initiation and repolarization are controlled by distinct potassium channel subtypes in CA1 pyramidal neurons. *J Neurosci* **19,** 8789-8798.

Golding NL, Kath WL & Spruston N. (2001). Dichotomy of action-potential backpropagation in CA1 pyramidal neuron dendrites. *J Neurophysiol* **86,** 2998-3010.

Golding NL & Spruston N. (1998). Dendritic sodium spikes are variable triggers of axonal action potentials in hippocampal CA1 pyramidal neurons. *Neuron* **21,** 1189-1200.

Harris KM & Stevens JK. (1989). Dendritic spines of CA 1 pyramidal cells in the rat hippocampus: serial electron microscopy with reference to their biophysical characteristics. *J Neurosci* **9,** 2982-2997.

Hines ML & Carnevale NT. (1997). The NEURON simulation environment. *Neural Comput* **9,** 1179-1209.

Holmes WR. (1989). The role of dendritic diameters in maximizing the effectiveness of synaptic inputs. *Brain Res* **478,** 127-137.

Jaffe DB & Carnevale NT. (1999). Passive normalization of synaptic integration influenced by dendritic architecture. *J Neurophysiol* **82,** 3268-3285.

Krijnse-Locker J, Parton RG, Fuller SD, Griffiths G & Dotti CG. (1995). The organization of the endoplasmic reticulum and the intermediate compartment in cultured rat hippocampal neurons. *Mol Biol Cell* **6,** 1315-1332.

London M, Meunier C & Segev I. (1999). Signal transfer in passive dendrites with nonuniform membrane conductance. *J Neurosci* **19,** 8219-8233.

Lörincz A, Notomi T, Tamás G, Shigemoto R & Nusser Z. (2002). Polarized and compartment-dependent distribution of HCN1 in pyramidal cell dendrites. *Nat Neurosci* **5,** 1185-1193.

Maccaferri G, Mangoni M, Lazzari A & DiFrancesco D. (1993). Properties of the hyperpolarization-activated current in rat hippocampal CA1 pyramidal cells. *J Neurophysiol* **69,** 2129-2136.

Magee JC. (1998). Dendritic hyperpolarization-activated currents modify the integrative properties of hippocampal CA1 pyramidal neurons. *J Neurosci* **18,** 7613-7624.

Magee JC. (1999). Dendritic lh normalizes temporal summation in hippocampal CA1 neurons. *Nat Neurosci* **2,** 508-514.

Magee JC & Cook EP. (2000). Somatic EPSP amplitude is independent of synapse location in hippocampal pyramidal neurons. *Nat Neurosci* **3,** 895-903.

Major G, Larkman AU, Jonas P, Sakmann B & Jack JJ. (1994). Detailed passive cable models of whole-cell recorded CA3 pyramidal neurons in rat hippocampal slices. *J Neurosci* **14,** 4613-4638.

Megias M, Emri Z, Freund TF & Gulyas AI. (2001). Total number and distribution of inhibitory and excitatory synapses on hippocampal CA1 pyramidal cells. *Neuroscience* **102,** 527-540.

Meyer E, Muller CO & Fromherz P. (1997). Cable properties of dendrites in hippocampal neurons of the rat mapped by a voltage-sensitive dye. *Eur J Neurosci* **9,** 778-785.

Rall W. (1959). Branching dendritic trees and motorneuron membrane resistivity. *Expl Neurol* **1,** 491-527.

Rapp M, Segev I & Yarom Y. (1994). Physiology, morphology and detailed passive models of guinea-pig cerebellar Purkinje cells. *J Physiol* **474,** 101-118.

Rapp M, Yarom Y & Segev I. (1992). The impact of parallel fiber background activity on the cable properties of the cerebellar Purkinje cells. *Neural Comput* **4,** 518-533.

Santoro B, Grant SGN, Bartsch D & Kandel ER. (1997). Interactive cloning with the SH3 domain of N-src identifies a new brain specific ion channel protein, with homology to Eag and cyclic nucleotide-gated channels. *Proc Natl Acad Sci U S A* **94,** 14815-14820.

Shelton DP. (1985). Membrane resistivity estimated for the Purkinje neuron by means of a passive computer model. *Neuroscience* **14,** 111-131.

Spacek J & Harris KM. (1997). Three-dimensional organization of smooth endoplasmic reticulum in hippocampal CA1 dendrites and dendritic spines of the immature and mature rat. *J Neurosci* **17,** 190-203.

Spruston N & Johnston D. (1992). Perforated patch-clamp analysis of the passive membrane properties of three classes of hippocampal neurons. *J Neurophysiol* **67,** 508-529.

Staff NP, Jung HY, Thiagarajan T, Yao M & Spruston N. (2000). Resting and active properties of pyramidal neurons in subiculum and CA1 of rat hippocampus. *J Neurophysiol* **84,** 2398-2408.

Stuart G & Spruston N. (1998). Determinants of voltage attenuation in neocortical pyramidal neuron dendrites. *J Neurosci* **18,** 3501-3510.

Stuart GJ, Dodt HU & Sakmann B. (1993). Patch-clamp recordings from the soma and dendrites of neurons in brain slices using infrared video microscopy. *Pflugers Arch* **423,** 511-518.

Thurbon D, Field A & Redman S. (1994). Electrotonic profiles of interneurons in stratum pyramidale of the CA1 region of rat hippocampus. *J Neurophysiol* **71,** 1948-1958.

Thurbon D, Luscher HR, Hofstetter T & Redman SJ. (1998). Passive electrical properties of ventral horn neurons in rat spinal cord slices. *J Neurophysiol* **79,** 2485-2502.

Williams SR & Stuart GJ. (2000). Site independence of EPSP time course is mediated by dendritic I(h) in neocortical pyramidal neurons. *J Neurophysiol* **83,** 3177-3182.

Tables

Table 1. Basic electrophysiological properties of CA1 pyramidal neurons.

	Control Mean ± SEM (*n*) Range	CsCl or ZD7288 Mean ± SEM (*n*) Range
R_N (MΩ)	54 ± 2 (31) 38 – 77	124 ± 9 (18) 59 – 213
V_{rest} soma (mV)	-67 ± 1 (31) -74 – -59	-71 ± 2 (18) -90 – -59
V_{rest} dend (mV)	-65 ± 1 (31) -71 – -56	-71 ± 2 (18) -85 – -63
Sag ratio	0.83 ± 0.01 (31) 0.73 – 0.91	0.98 ± 0.01 (18) 0.94 – 1.00

Table 2. Membrane time constant estimates in the presence of 5 mM CsCl (Mean ± SEM).

	Soma (*n*)	Dendrite (*n*)
τ_{ON} (ms)	44 ± 4 (19)	43 ± 4 (19)
Range	15 – 55	15 – 52
τ_{OFF} (ms)	42 ± 4 (19)	43 ± 4 (19)
Range	14 – 47	15 – 49
τ_{SHORT} (ms)	38 ± 3 (14)	39 ± 3 (14)
Range	14 – 45	15 – 48

Table 3. Uniform and nonuniform membrane resistivity model parameters.

		R_i (Ωcm)	R_m *soma* (Ωcm^2)	R_m *dend* (Ωcm^2)	C_m (μF/cm^2)	RMS error (mV)
Uniform	Cell 1	261	39,880	39,880	1.02	0.167
	Cell 2	225	25,700	25,700	1.40	0.249
	Cell 3	198	16,054	16,054	1.86	0.422
Nonuniform	Cell 1	218	62,901	31,916	1.06	0.106
	Cell 2	176	125,610	17,853	1.43	0.170
	Cell 3	139	74,697	10,216	2.02	0.406

Legends

Figure 1. Morphology and voltage responses of modeled CA1 pyramidal neurons. *A*, Morphological reconstruction of the three neurons used in this study, with electrode positions in each recording indicated schematically (and providing scale for each neuron). The dendritic recording distances indicated were measured during the experiment. Actual distances in the NEURON reconstructions are about 10% longer due to the indirect path between electrodes. *B*, Somatic (large) and dendritic (small) voltage responses to somatic current injections in control ACSF. *C*, Somatic and dendritic voltage responses to somatic current injections in the presence of 5 mM CsCl, which completely blocks the "sag." Scale bar is the same as in *B*. The current injection protocol is indicated below the leftmost set of traces. The long pulse was –30 to –50 pA for 400 ms, with amplitude adjusted to give a < 5 mV response in control ACSF (*B*); the same amplitude was used in CsCl (*C*). The short pulse was 1 ms long, and -1.5 nA in amplitude.

Figure 2. Somatic to dendritic steady-state voltage attenuation. The ratio of the dendritic steady-state voltage response (long current pulse) to the somatic steady-state amplitude is plotted as a function of distance in control (open circles, $n = 34$) or with H current blocked (5 mM CsCl, filled circles, $n = 16$; 50-100 µM ZD7288, filled triangles, $n = 5$). Data were fit with a linear function. The 50% attenuation distance in control was 238 µm and in 5 mM CsCl was 409 µm (extrapolated).

Figure 3. Fits of long and short-current pulse responses using uniform and nonuniform membrane resistance (R_m) models. For nonuniform fits, R_m was allowed to vary as a function of distance, using a sigmoidal function (see Methods). Raw data are indicated in black, and fits are indicated in red. *A,B,* Best fits using uniform R_m (*A*) and nonuniform R_m (*B*). *C,* The R_m gradient, normalized to the somatic R_m, as a function of distance in each of the cells for the apical dendrite. For parameter values of these models see Table 3.

Figure 4. Fits of voltage responses in models containing uniform and nonuniform H conductance. Models of the best fits using nonuniform R_m were used as the underlying passive model. G_h varied as a sigmoidal function of distance (see Methods). Fits were weighted to ensure a match of the steady-state voltage response. Raw data are indicated in black, and fits are indicated in red. *A,* Best fits of the data using models with uniform G_h and nonuniform R_m. The mean square error MSE for cell 1 was 0.141 mV; for cell 2, MSE = 0.151; for cell 3, MSE = 0.155. *B,* Best fits of the data using models with nonuniform G_h and nonuniform R_m. The MSE for cell 1 was 0.115; for cell 2, MSE = 0.147; for cell 3, MSE = 0.079. *C,* The H conductance gradient, normalized to the somatic G_h value, as a function of distance in each of the cells for the main apical dendrite sections. Somatic G_h for cel1 1 was 2.17 pS/μm^2, for cell 2, 16.8 pS/μm^2, for cell 3, 0.22 pS/μm^{2}s.

Figure 5. Comparison of steady-state attenuation of models having a nonuniform R_m with measured voltage attenuation. *A*, Voltage attenuation with H conductance blocked. Figure at right shows steady-state voltage attenuation for cell 3, with the color map indicating hyperpolarizing voltage changes of 3 mV (blue) to less than 0.3 mV (red). The closed circles and triangles are the same CsCl and ZD7288 attenuation data as from Figure 2. *B*, Voltage attenuation with H conductance present. Figure at right shows steady-state voltage attenuation for cell 3, with the color map indicating hyperpolarizing voltage changes of 2 mV (blue) to less than 0.2 mV (red). The ratio of the dendritic to the somatic voltage response (long somatic current injection) is plotted for each section of the primary apical dendrite. Each line corresponds to one model cell. The open circles are the same control attenuation data as from Figure 2.

Figure 6. Attenuation of EPSPs as they propagate from the dendrite to the soma. *A*, Schematic diagram of the experiments and simulations to measure EPSP attenuation. EPSPs were evoked via a stimulating electrode placed in stratum lacunosum-moleculare and recorded in the dendrite and the soma. For simulations, 40 unitary synaptic inputs in stratum lacunosum-moleculare (as indicated schematically by dots on dendrites) were modeled with a fast conductance increase of 0.1 nS each (0.5 ms rise, 5 ms decay), yielding composite somatic EPSPs of 3.6, 2.0, and 1.8 mV (cells 1, 2, and 3, respectively) at the soma. *B*, EPSP attenuation ($V_{soma}/V_{dendrite}$) is plotted as a function of distance of the dendritic recording for the six simultaneous somatic/dendritic recordings (circles) and for the three models (lines represent attenuation measured from numerous dendritic locations; the cell numbers corresponding to each line are indicated). The inset shows representative EPSPs recorded simultaneously from the soma and dendrite (305 μm). All simulations and recordings were performed with H conductance present (not blocked).

Figure 7. Simulations of EPSP attenuation for various synaptic locations. Nonuniform R_m and G_h models for cell 3 were used in these simulations. The synaptic conductance was 1 nS with a rise time constant of 0.5 ms and a decay time constant of 5 ms. *A*, The five synapse locations are indicated by the colored markers (basal site at 135 µm, green; proximal site at 290 µm, blue; side branch site at 322 µm, purple; distal apical at 583 µm, orange; and a second distal apical at 730 µm, yellow) and the somatic and dendritic recording sites are indicated by the electrode cartoons (dendritic recording electrode at 365 µm). *B*, Bar graph showing the amplitude of the somatic EPSP for the five synapses. Results are presented for models with and without H conductance (darker bars and lighter bars, respectively). *C*, Example of simulated EPSPs in response to activation of a distal apical synapse (orange marker in A) and measured at the synapse (orange), the dendritic recording site (black), and at the soma (red). In this example the EPSP attenuates 26 fold between the synapse and the soma.

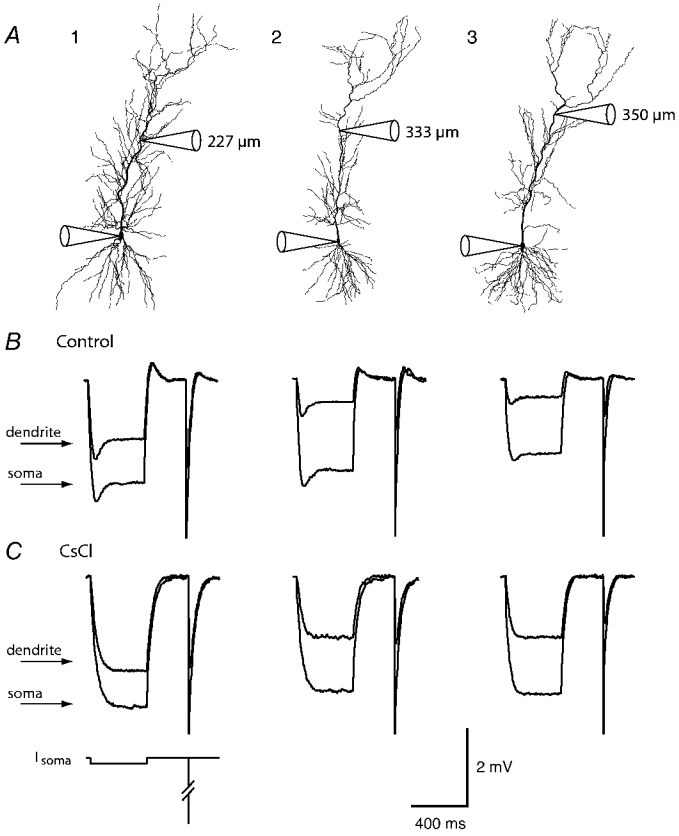

Golding et al., Figure 1

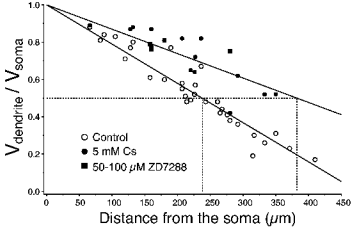

Golding et al., Figure 2

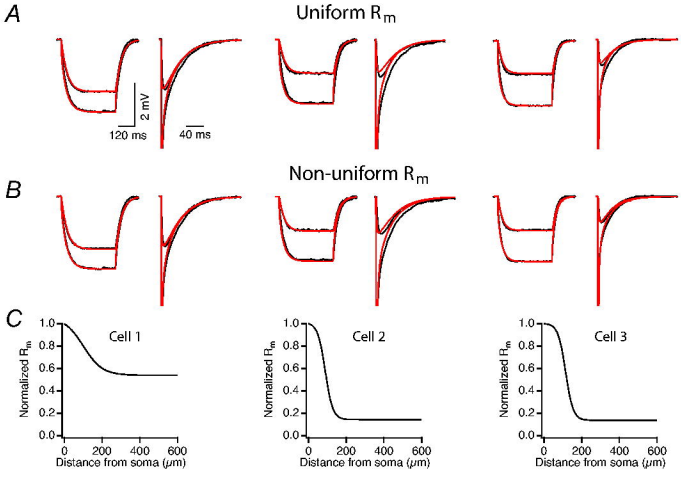

Golding et al., Figure 3

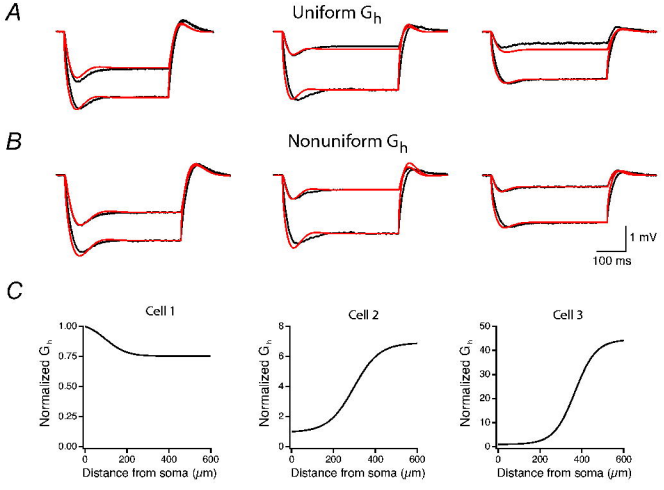

Golding et al., Figure 4

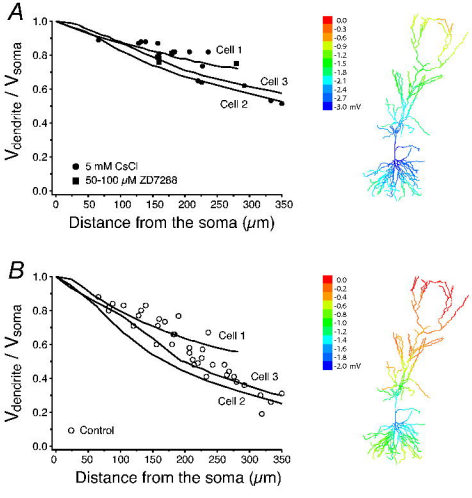

Golding et al., Figure 5

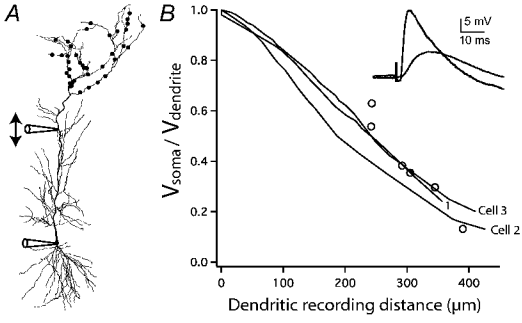

Golding et al., Figure 6

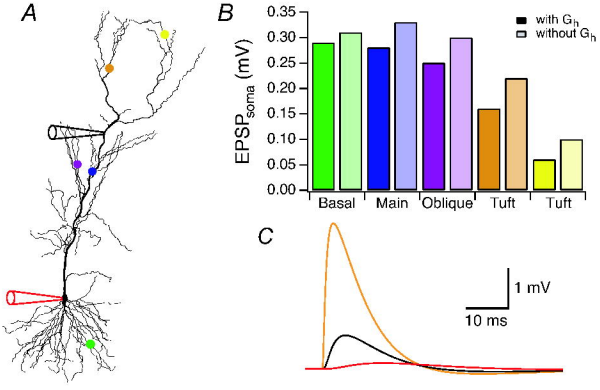

Golding et al., Figure 7